Ionization scaling law for ions colliding with elliptical Rydberg hydrogen targets

Marc Ward, Thomas Cooper, Zach Wilbanks, and Kevin Cornelius
Ouachita Baptist University, Arkadelphia, Arkansas 71998, USA
(Received 5 April 2012; published 28 June 2012)

The classical trajectory Monte Carlo (CTMC) method has been used to model fully stripped ions of He, C, Ar, and Kr colliding with aligned elliptic Rydberg hydrogen in various excited initial n states. CTMC cross sections from target eccentricities of -0.99 to 0.99 and reduced ion velocities ranging from 5 to 40 were used to develop an ionization scaling law as a function of reduced velocity v^*, initial n state, projectile charge q, and initial electron eccentricity ε. The nonelliptic part of our scaling law has been compared to other existing ionization models and found to be in very good agreement.

DOI: 10.1103/PhysRevA.85.064701 PACS number(s): 34.10.+x, 34.50.−s

I. INTRODUCTION

Ion-Rydberg atom collisions have been important systems to study because they provide a good probe of astronomical phenomena as well as ultracold plasmas [1–3]. Radio astronomers have found highly excited or Rydberg atoms in nebulae, diffuse interstellar gas, supernova remnants, and the coronas of comets [4]. Most recently, the interactions between Rydberg atoms and metal surfaces have been of interest [5,6]. Being able to identify the formation and decay likelihood of Rydberg atoms can help in the determination of the physics present in these particular areas. In most of these active areas of research, electron capture involving the Rydberg atoms has been the primary focus, while other interactions such as charge exchange or ionization receive much less attention. In this report, we wish to look at the ionization of a Rydberg target by many different fully stripped ions in an attempt to provide a single function to predict the total ionization cross sections between an incident ion projectile and a Rydberg target in a predetermined quantum state at very high collision energies.

II. THEORY

Absolute ionization cross sections have been calculated for fully stripped ions colliding with hydrogen Rydberg targets in various initial excited and elliptical states using the well-known classical trajectory Monte Carlo (CTMC) method [7,8]. The particular CTMC approach used in this Brief Report is well documented in the literature [9] and will only be briefly outlined here.

The collision system contains an incident ion and an electron bound to a hydrogen atom in a predetermined circular or elliptic Keplerian orbit corresponding to a Rydberg state with a principle quantum number n. The orbital plane of the electron, located in the xy geometric plane, is oriented so that the orbital angular momentum vector of the electron (L_z) points along the $+z$ axis. As such, the incident ion sees the entire orbital plane of the electron upon its approach. The eccentricity of the orbit is defined such that a circular orbit ($\varepsilon = 0$) is centered on the target nucleus. When the orbit is stretched elliptically, the target nucleus is located at one focus while the orbit is elongated along the x axis, with $\varepsilon > 0$ representing a stretching in the $+x$ direction and $\varepsilon < 0$ in the $-x$ direction. In practice, *any* arbitrary axis in the xy plane could have been chosen as the elongation axis since the orbital angular momentum vector of the electron is always parallel to the momentum vector of the incident ion regardless of the alignment axis chosen. Figure 1 shows a view of the target collision system from the point of view of the incoming ion beam as it approaches the target perpendicular to the orbital plane of the electron along with a visual depiction of the elliptically stretched orbits.

The main collision parameters are the charge of the projectile ion (q), the eccentricity of the orbit (ε), the principle quantum number of the bound electron (n), and the velocity of the incoming ion (v_{ion}). Going forward, a reduced velocity (v^*) will be used for convenience and written in terms of the projectile velocity and the velocity of the orbital electron as

$$v^* = \frac{v_{\text{ion}}}{v_e}. \tag{1}$$

This relation can also be written in terms of the orbital velocity of the Rydberg electron as

$$v^* = n v_{\text{ion}}. \tag{2}$$

Once all the initial conditions of the system are determined, the system is propagated classically by numerically solving Hamilton's equation of motion for the three-body system. The absolute ionization cross sections (in cm^2) are determined using

$$\sigma = \left(\frac{N_i}{N}\right)\pi a_o^2 b_{\max}^2, \tag{3}$$

where N_i is the total number of ionization events, N is the total number of trajectories, a_o is the Bohr radius, and $b_{\max}$ is the largest value of the impact parameter for which an ionization event occurs at a particular reduced velocity. In an effort to obtain good and consistent results with small statistical errors, the number of trajectories for each collision type was adjusted in order to produce ∼1500 ionization events, since the errors are on the order of

$$\Delta\sigma \approx \frac{1}{\sqrt{N_i}}. \tag{4}$$

III. DATA

Individual ionization cross sections for He^{++} at a reduced velocity of $v^* = 5$, C^{6+} at $v^* = 10$, Ar^{18+} at $v^* = 15$, and Kr^{36+} at $v^* = 20$ were calculated for target excitations of $n = 4$, 16, 25, and 50 with eccentricities ranging from -0.99 to 0.99.

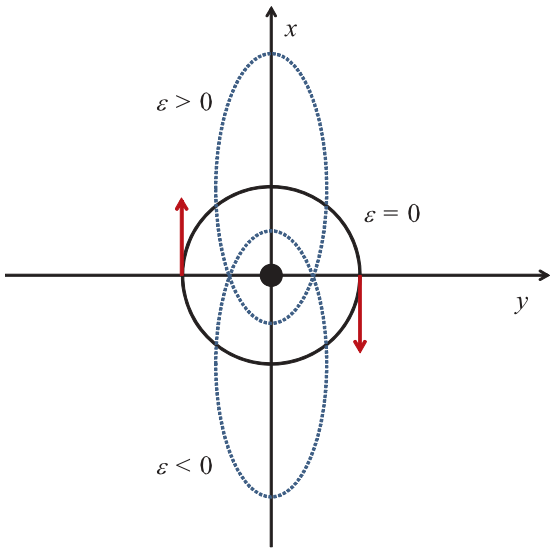

FIG. 1. (Color online) The Rydberg target as viewed by the incident ion with the $+z$ axis extending into the page. The eccentricity $\varepsilon = 0$ denotes a circular orbit about the hydrogen core and $\varepsilon > 0$ and $\varepsilon < 0$ represent a stretching of the orbit along the $+x$ and $-x$ axis, respectively. The arrows indicate the orbital direction of the electron about the nucleus.

From the results plotted in Fig. 2, a few initial observations can be made. First, the cross sections form nice symmetric bands at each principle quantum n value due to the symmetry of the collision. Second, the total cross sections increase with n for all projectiles as the energy of the ion can more easily remove the weaker bound electrons in the larger orbits. Lastly, the cross sections also increase as the charge of the ion increases due to the additional attractive Coulomb strength of the ion.

A more detailed look at Fig. 2 reveals that the ionization cross sections at large eccentricities ($|\varepsilon| \geqslant 0.9$) begin to decrease slightly as the electron orbit becomes more elongated. For these highly elliptic orbits, the atom behaves like an electric dipole and classical ionization becomes strongly suppressed for large collision speeds and large impact parameters as it is increasingly more difficult for the ion to impart enough momentum to the electron in the forward direction to liberate it from the host nucleus [9]. This is a known limitation of the CTMC in calculating ionization cross sections with dipolelike transitions driven by soft collisions with small momentum transfers [10].

IV. RESULTS

To better organize the ionization data, a scaling law of the form

$$\sigma_{\text{reduced}} = \frac{\sigma_{\text{ion}}}{q^a (v^*)^b n^d} \tag{5}$$

was used to reduce all the ionization cross sections in Fig. 2. Initially, the cross sections were reduced independently of n and it was found empirically that the values of 2 and -1.98, for the parameters a and b, respectively, provided the best

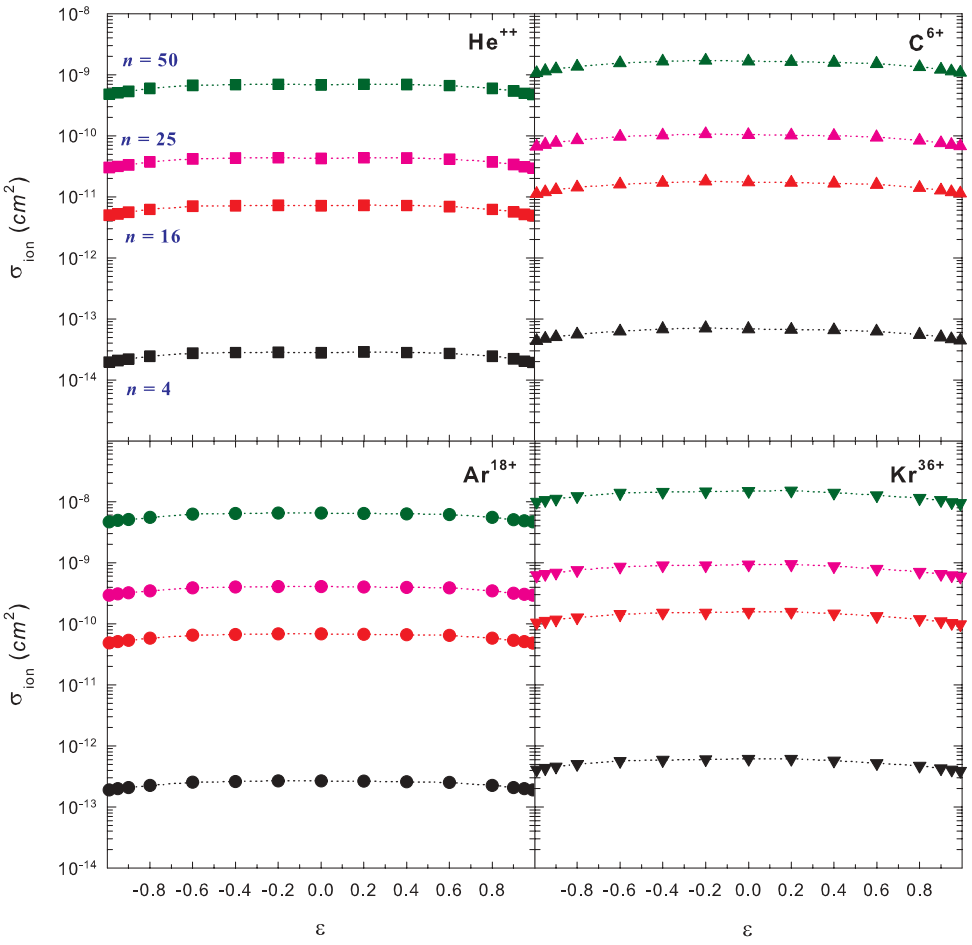

FIG. 2. (Color online) Total ionization cross sections are shown for He^{++} at a reduced velocity of $v^* = 5$, C^{6+} at $v^* = 10$, Ar^{18+} at $v^* = 15$, and Kr^{36+} at $v^* = 20$ for initial target excitations of $n = 4, 16, 25$, and 50. Each projectile's cross sections are plotted as a function of eccentricity (ε) ranging from -0.99 to 0.99.

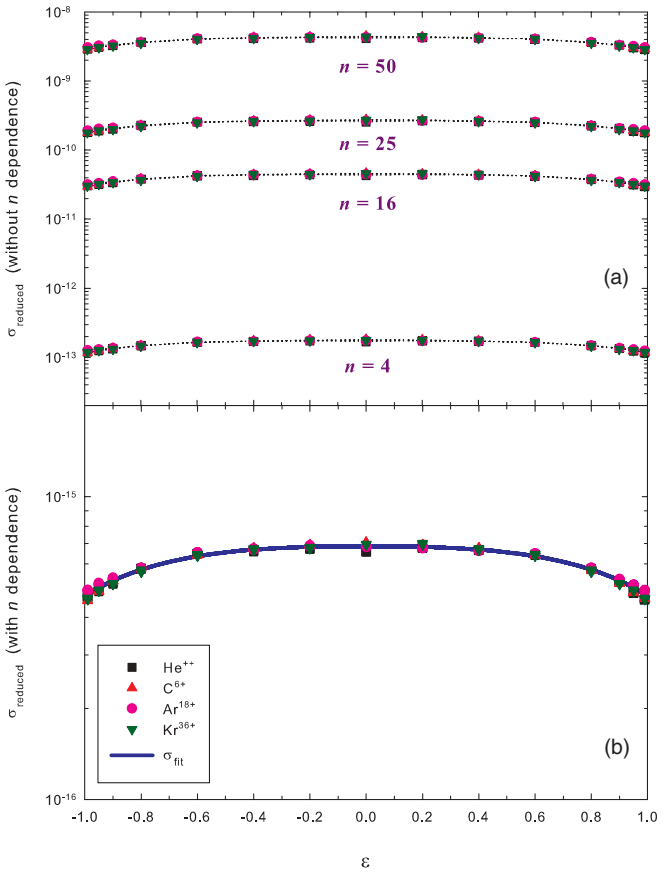

FIG. 3. (Color online) (a) Reduced total ionization cross sections for all projectiles without n dependence [Eq. (6)]. (b) Same cross sections as in (a) but now including n dependence [Eq. (7)]. The solid (blue) line fitted to the data is $\sigma_{\rm fit}$ [Eq. (9)].

results. Plots of the data under the reduction

$$\sigma_{\rm reduced} = \frac{\sigma_{\rm ion}}{q^2(v^*)^{-1.98}} \tag{6}$$

are shown in Fig. 3(a). The scaling law produces very nice reduced curves across all eccentricities, each collapsing along corresponding n values. When including the cross sections' dependence on n, the optimal value for the exponent d was found to be 4, which is consistent with other ion-Rydberg collision scaling laws using reduced velocities [11]. Using

$$\sigma_{\rm reduced} = \frac{\sigma_{\rm ion}}{q^2(v^*)^{-1.98}n^4}, \tag{7}$$

all of the scaled independent n data curves in Fig. 3(a) reduced down to a single unified curve [Fig. 3(b)].

A total cross-section function involving all the parameters of the collision system of the form

$$\sigma_{\rm fit} = Cq^2(v^*)^{-1.98}n^4(1 - A|\varepsilon|^f)^g \tag{8}$$

was used to model the reduced universal data curve in Fig. 3(b). Analysis that produced the best empirical fit involving the remaining unknown coefficients and exponents in (8) led to a final cross-section function given by

$$\sigma_{\rm fit} = 6.85 \times 10^{-16}q^2(v^*)^{-1.98}n^4(1 - 0.48|\varepsilon|^{2.7})^{0.58}. \tag{9}$$

This function is plotted as the solid (blue) curve in Fig. 3(b). This expression provides an outstanding reproduction of the reduced ionization cross sections. It is possible and perhaps even preferable to rewrite this function in terms of the initial velocity of the incident ion and not the reduced velocity for quicker analysis. In that case, v^* is replaced with the expression in Eq. (2) and the total cross-section function in Eq. (9) becomes

$$\sigma_{\rm fit} = 6.85 \times 10^{-16}q^2v_{\rm ion}^{-1.98}n^{2.02}(1 - 0.48|\varepsilon|^{2.7})^{0.58}. \tag{10}$$

It should be pointed out that while only data as low as $n = 4$ have been used in the determination of our scaling law, various sample calculations of cross sections at lower initial states of $n = 1$ to 3 were performed and were still found to be correctly and accurately modeled by Eq. (9).

Equation (9) can be compared to other existing scaling laws, in part, if it is rewritten as

$$\sigma_{\rm fit} = \sigma_o(v^*,n,q)F(\varepsilon), \tag{11}$$

with

$$\sigma_o(v^*,n,q) = 6.85 \times 10^{-16}q^2(v^*)^{-1.98}n^4, \tag{12}$$

representing the $\varepsilon = 0$ (circular orbit) cross-section component for all collisions and

$$F(\varepsilon) = (1 - 0.48|\varepsilon|^{2.7})^{0.58}, \tag{13}$$

which contains all the elliptical influence on the total cross section. In this separate form, it can be seen that the first part of $\sigma_{\rm fit}$, Eq. (12), has nearly the same exact form as the Bohr formula for ionization cross sections originally derived by Thomas [12]:

$$\sigma_{\rm Bohr}(v^*,n,q) = 3.519 \times 10^{-16}q^2(v^*)^{-2}n^4. \tag{14}$$

When you take into account that an electron with nonzero orbital velocity requires less energy transfer for ionization, the total ionization cross section becomes approximately 5/3 larger for a hydrogen target [13]. This yields a modified Bohr formula cross-section function of

$$\sigma^*_{\rm Bohr}(v^*,n,q) = 5.865 \times 10^{-16}q^2(v^*)^{-2}n^4. \tag{15}$$

Two additional ionization cross-section models that prove more accurate at very high-energy collisions, one developed by Bethe and the other by Gryzinski [13], are given by:

$$\sigma_{\rm Bethe}(v^*,n,q) = 1.99\times10^{-16}q^2(v^*)^{-2}n^4[2.2279 + \ln(v^*)], \tag{16}$$

and

$$\sigma_{\rm Gryz}(v^*,n,q) = 3.519 \times 10^{-16}q^2(v^*)^{-2}n^4 \times [1 + 0.667\ln(2.7 + v^*)]. \tag{17}$$

When compared to our model and the Bohr ionization model, other than the additional logarithmic terms, they all have the same exact form, but with differing coefficients. The logarithmic terms are limiting forms of more complex functions involving v^* and are a result of large impact parameter ionizations to the total cross section at very high energies. Classically, ionization under these conditions is forbidden because the energy transferred by the projectile to the electron

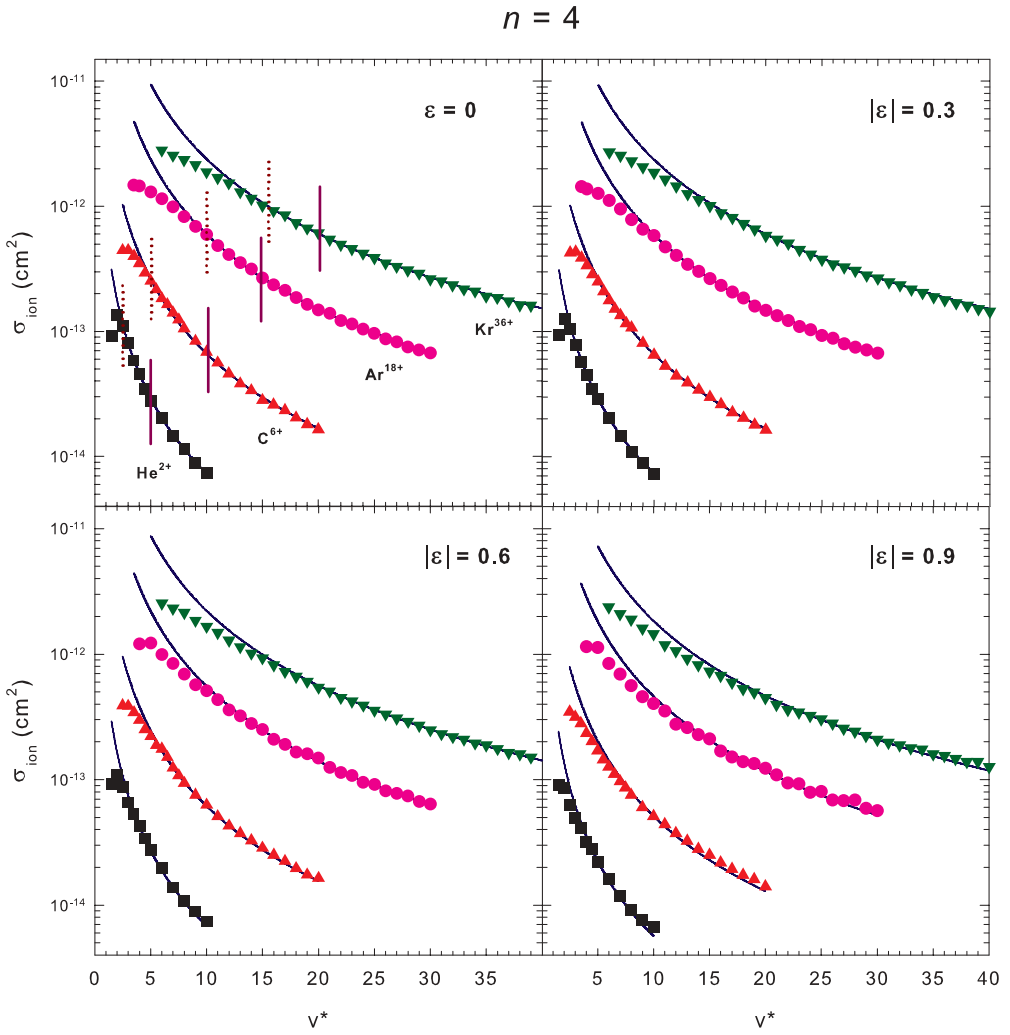

FIG. 4. (Color online) Total ionization data for all four incident ions of various eccentricities as a function of reduced velocity for a Rydberg target in an excitation state of $n = 4$ only. The solid (blue) curves through the data are produced by Eq. (9) using initial parameters unique to each respective collision system. The solid vertical lines in the upper left frame ($\varepsilon = 0$) act as a reference to indicate the original collision speeds used to calculate the initial ionization cross sections shown in Fig. 2. The vertical dotted line represents the location where an application of the current cross-section fitting function [Eq. (9)] becomes valid as determined by Eq. (18).

is less than the ionization potential. However, ionization is still possible from the standpoint of quantum mechanics due to diffraction [14]. As a result, quantum mechanical cross sections are larger than classically determined cross sections at high energies [13]. For these high-energy collisions, it would seem plausible to combine either Eq. (16) or (17) with $F(\varepsilon)$ from Eq. (13) to provide a first-order, elliptical ionization cross-section model.

For another test of the validity of Eq. (9), additional ionization cross sections were calculated as a function of reduced velocities for eccentricities of 0.0, 0.3, 0.6, and 0.9 for $n = 4$ and 25 for each projectile ion. Since the cross sections are symmetric about $\varepsilon = 0$, only positive eccentricities were used. As seen in Figs. 4 and 5, the cross-section model (σ_{fit}) predicts the CTMC elliptical ionization cross sections with very good agreement after reaching a specific reduced velocity (marked with a dashed vertical line), which is a value unique to each ion. Only at the highest eccentricities does the fit begin to show some difficulty (as seen for $|\varepsilon| = 0.9$). Warning signs for this potential difficultly were noted earlier in Fig. 2 and are more apparent in the reduced universal curve in Fig. 3(b) as the cross sections at large ε were not as tightly grouped as at other eccentricities. As the orbit becomes increasingly elongated ($|\varepsilon| > 0.9$), the calculated cross sections not only begin to decrease rapidly, but no longer appear to scale in the same manner as the less-elliptical orbits.

Investigations were performed into that point mentioned earlier at which the cross-section model (σ_{fit}) begins to correctly reflect the calculated CTMC cross sections for every projectile and initial n value (dashed vertical line). It was found that the reduced velocities where the calculated cross sections and the empirical curve fit start to coincide was independent of n and only a function of projectile charge (q) and the initial orbital eccentricity (ε). For each collision system, the starting reduced velocity when the ionization data can be correctly reproduced by σ_{fit} was found to be determined by

$$v^*(q,\varepsilon) = 1.614q^{0.631}(1 + |\varepsilon|^{1.1})^{0.4}. \tag{18}$$

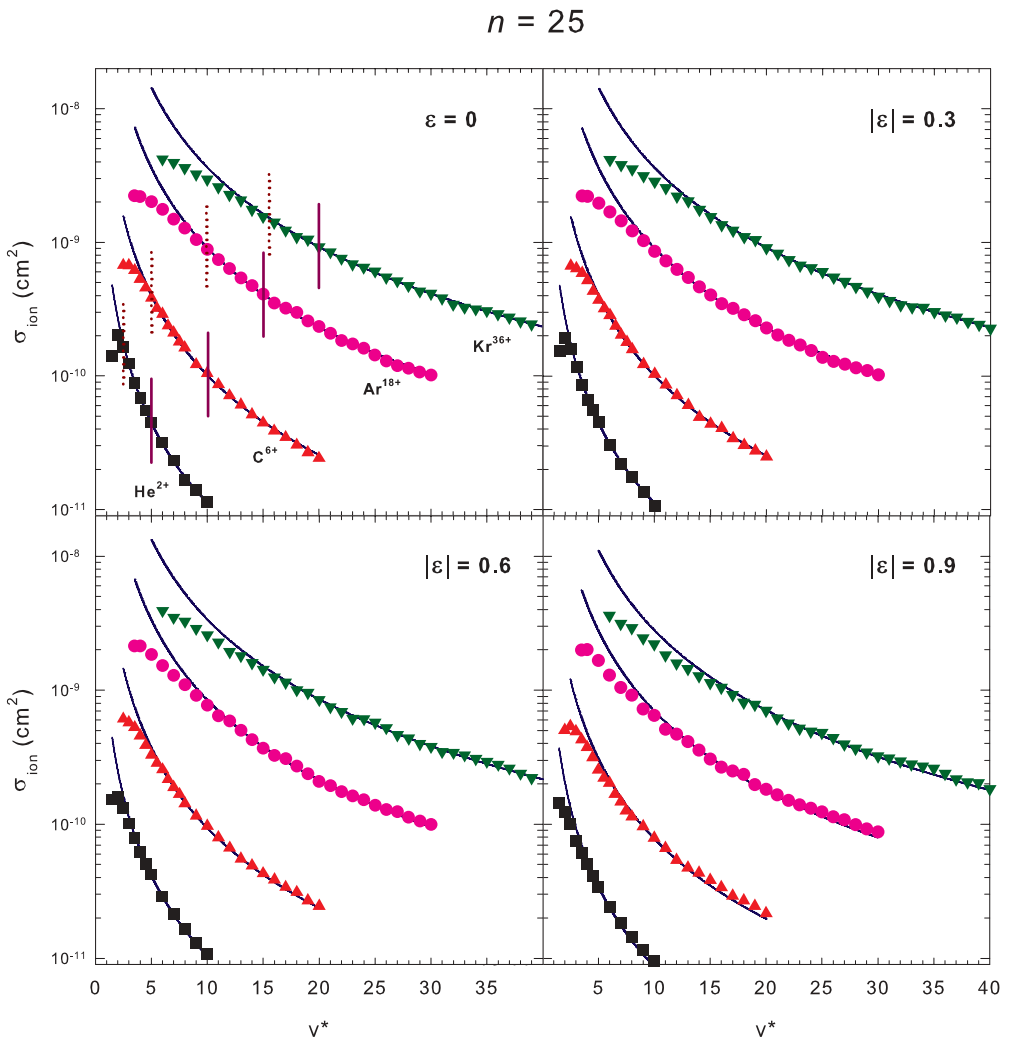

FIG. 5. (Color online) Same as Fig. 4 except for $n = 25$.

For illustration purposes, the circular case ($\varepsilon = 0$) in Figs. 4 and 5 have the initial velocities used to determine the original scaling law marked (solid vertical lines) along with the starting velocities where Eq. (11) indicates it is valid to start applying Eq. (9) (dashed vertical line). Analysis of Eq. (11) showed it correctly predicted the starting v^* values for all eccentricities from -0.8 to 0.8. For $|\varepsilon| \geqslant 0.9$, it becomes difficult to determine an initial point where the curve fit model and the data begin to converge since the two are not well unified and look more like a crossing than a merging.

V. CONCLUSION

In this paper, CTMC ionization data for various fully stripped ions colliding with Rydberg targets has been presented. It has been shown that the cross sections for all the systems can be scaled down to a single universal curve, which compares very well to other theoretically developed models. The final reduced data curve was then fitted with an empirical function based on the initial collision parameters with great success, but only for collision speeds beyond a minimum threshold based on ion charge and eccentricity. While the presented model works extremely well for most collision combinations, it did show some discrepancy with the data for extremely eccentric orbits ($|\varepsilon| \geqslant 0.9$), which was not too surprising since it is in a region of known difficulty for classical approaches.

ACKNOWLEDGMENTS

The authors would like to thank the Ouachita Baptist Physics Department for the use of their computing resources and Dr. J. D. Patterson for his continued personal and financial support of undergraduate research.

[1] M. R. Flannery and D. Vrinceanu, Phys. Rev. A **68**, 030502(R) (2003).

[2] H. Tawara, in *The Physics of Multiply and Highly Charged Ions*, edited by F. J. Currell, Vol. 1 (Kluwer Academic, Dordrecht, 2003), p. 103.

[3] X. Lu, Y. Sun, and H. Metcalf, Phys. Rev. A **84**, 033402 (2011).

[4] C. M. Lisse, K. Dennerl, J. Englhauser, M. Harden, F. E. Marshall, M. J. Mumma, R. Petre, J. P. Pye, M. J. Ricketts, J. Schmitt, J. Trümper, and R. G. West, Science **274**, 205 (1996).

[5] J. Sjakste, A. G. Borisov, and J. P. Gauyacq, Phys. Rev. A **73**, 042903 (2006).
[6] N. N. Nedeljković and D. K. Božanić, Phys. Rev. A **81**, 032902 (2010).
[7] I. C. Percival and D. Richards, Adv. At. Mol. Phys. **11**, 1 (1975).
[8] R. E. Olson and A. Salop, Phys. Rev. A **16**, 531 (1977).
[9] K. R. Cornelius, J. Wang, and R. E. Olson, J. Phys. B **31**, 4367 (1998).
[10] C. O. Reinhold and J. Burgdörfer, J. Phys. B **26**, 3101 (1993).
[11] J. Wang, R. E. Olson, K. R. Cornelius, and K. Tökési, J. Phys. B **29**, L537 (1996).
[12] J. J. Thompson, Philos. Mag. **23**, 449 (1912).
[13] I. D. Kaganovich, E. Startse, and R. C. Davidson, New J. Phys. **8**, 278 (2006).
[14] H. A. Bethe and R. Jackiw, *Intermediate Quantum Mechanics*, 2nd ed. (Benjamin-Cummings, New York, 1968).